

https://dspace.org/

The development of a tough high chronmium ferritic stainless steel

Hermanus, Mavis Ann

2015-01-27
http://hdl.handle.net/10539/16775

Downloaded from a DSpace repository. https://dspace.org/

4.5 OPTICAL METALLOGRAPHY

Detailed optical studies were carried out with a view to gaining greater understanding of the relationship between microstructure and mechanical properties. Grain size was measured and inclusion size and morphology were determined.

4.5.1 Grain size

The grain size of some of the alloys studied is given in table 4.11

Table 4.11 Grain size of selected alloys.

Alloy	Grain size µm	Room temperature impact energy (JOULES)
V2/1/2	150-180	167
V3/2	180	210
V2/2/2	180	212
V4/0	180	6*
V4/0,1 (a)	90	6*
V4/0,1(b)	250-300	140

* embrittled alloys

From this table it can be seen that although the grain size of the alloy V4/0 was similar to that of the V2 and V3 alloys. and that of V4/0,1 (a) was considerably smaller, both of these materials had very low impact energies. The source of the embrittlement was clearly evident in their microstructure, which exhibited heavy stringers of σ-phase. Although these precipitates inhibited grain growth, they were nevertheless extremely deleterious to toughness.

In contrast, the tough V4/0,1 (b) alloy contains little trace of σ after heat treatment. The room temperature impact energy of this alloy is lower than that of the V2 and V3 alloys and correlated with a larger grain size. However, the apparent, very simple

relationship between grain size and toughness (a smaller grain size corresponding to a greater toughness) was again obscured by the fact that the interstitial content of V4/0,1 (540ppm) was higher than that of the V2 and V3 alloys (380-450ppm).

The V2 and V3 alloys themselves illustrate the complex interplay between grain size, interstitial impurity levels, the amount of REM added and toughness. In particular two unexpected results were obtained. The alloys V2/1/2 and V2/2/2 contained similar amounts of impurities (450ppm), yet V2/1/2 which had a smaller grain size had a poorer toughness at ambient temperature than V2/2/2 (to which 0,3% REM had been added). In addition, the V3/2 alloy (0,15 REM) with an identical grain size to V2/2/2 and which also had the lowest interstitial content of all the alloys studied (380ppm) did not have the highest impact toughness at room temperature.

The evidence thus suggests that although grain size may be an important variable in determining the toughness of the alloys, the level of interstitial impurity also plays an important and sometimes dominant role.

4.5.2 Interstitial precipitation

Since previous research has clearly associated interstitials with embrittlement, the condition of the interstitial elements (in solution or precipitated) their distribution and morphology were carefully monitored in this study. A quantitative analysis of the inclusions (Section 4.9) complements the qualitative observations given in this section.

4.5.2.1 Alloys which do not contain REM

In the alloys which do not contain rare earths, two types of inclusions were observed; blocky and needle-like. These were identified as (Fe and Cr) oxides using electron microprobe analysis. A few of the inclusions contained carbon and nitrogen. These were generally indistinguishable from the oxides in

appearance. They are also grey and blocky. Typical examples of the interstitial inclusions are shown in Figures 4.13(a to d).

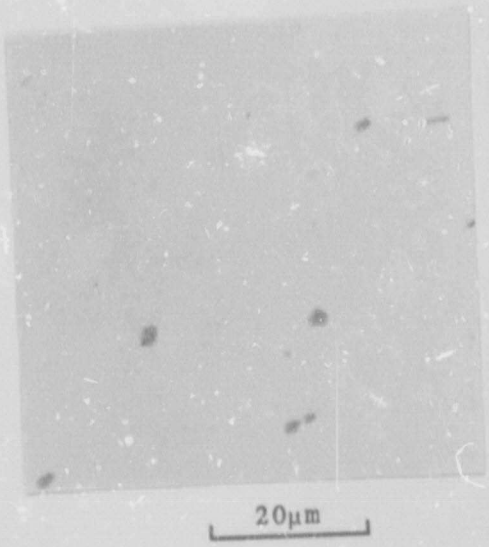
In general the blocky inclusions were unevenly distributed in the ductile alloys. They occur intragranularly although a few were found on the grain boundaries. Occasional dense clumps of inclusions were observed. In brittle alloys, the blocky inclusions were more densely and evenly distributed. Needle-like inclusions on the other hand, were very few in number in all the alloys. These occurred singly, in strings or in clumps (and were also found in the alloys which did contain REM). They do not seem therefore, to be related to either REM content, or ductile or brittle behaviour in any consistent way.

The precipitates were not all the same size; while most are fairly small, a few large inclusions were evident.

4.5.2.2 Alloys which contain REM

When REMs were added to the Fe-40Cr alloys the blocky inclusions increased in size and became spheroidal. This effect is illustrated in Figures 4.14 and 4.15. The ductile REM-containing alloys (V3/2, and V4/3,1) contained fewer inclusions than the ductile alloys which have no REM content. REM additions in excess of the predicted optimum (0,6 and 0,9%) resulted in embrittlement. This was due to an increase in the number of inclusions both at grain boundaries (Figure 4.16) and within the grains (Figure 4.17).

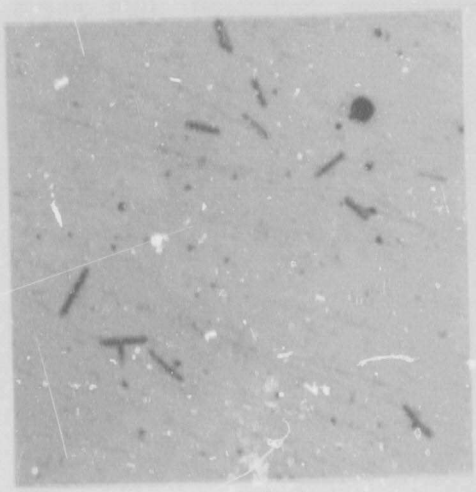
Electron microprobe analysis showed that the rounded inclusions were oxides containing iron, chromium and rares earths.



(a)



(b)



(c)



(d)

Figure 4.13 Typical examples of inclusions and their distribution.
a) Blocky inclusions in V2/1/2 alloy. Unetched condition.
b) Oxide inclusions at the grain boundary (V1/2). Glyceregia etch.
c) A clump of needle-like inclusions (V2/1/2). Glyceria etch.
d) Isolated needle-like inclusions (V2/2/2). Glyceria etch.

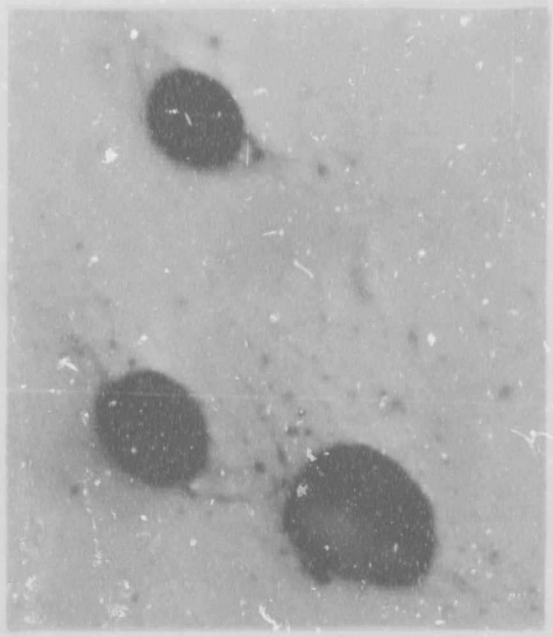


Figure 4.14 Rounded inclusions in the V3/2 alloy, which contains 0,15% REM. Unetched condition.

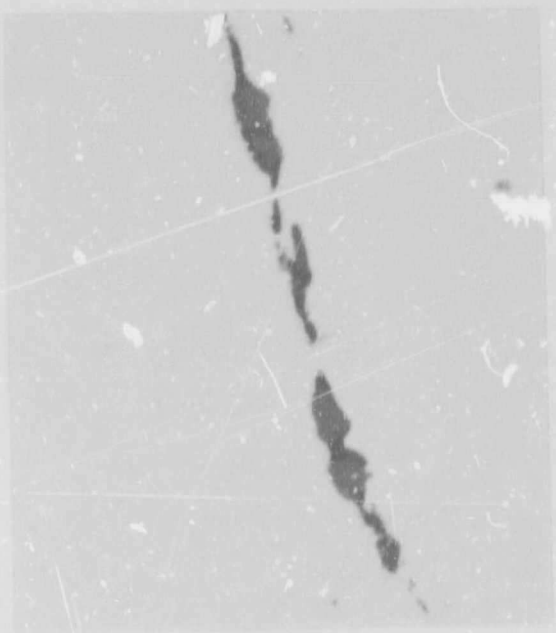


Figure 4.15 A string of partially spheroidised, angular inclusions (V4/0.10). Unetched condition.

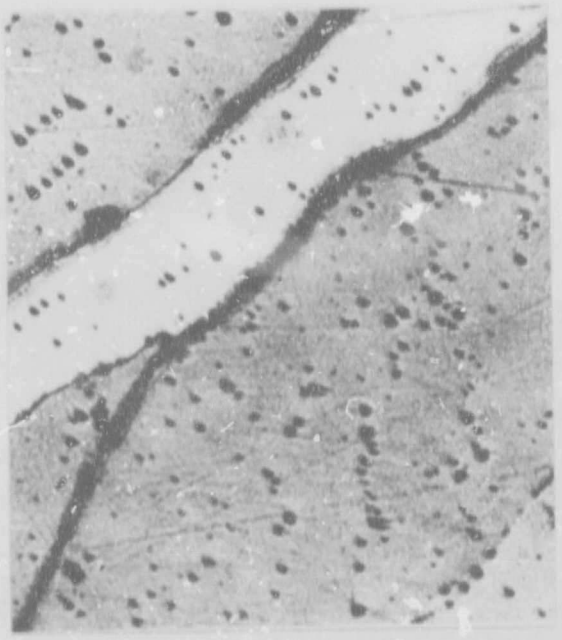


Figure 4.16 REM oxide inclusions. Section parallel to the rolling direction (V2/S). Glyceregia etch.

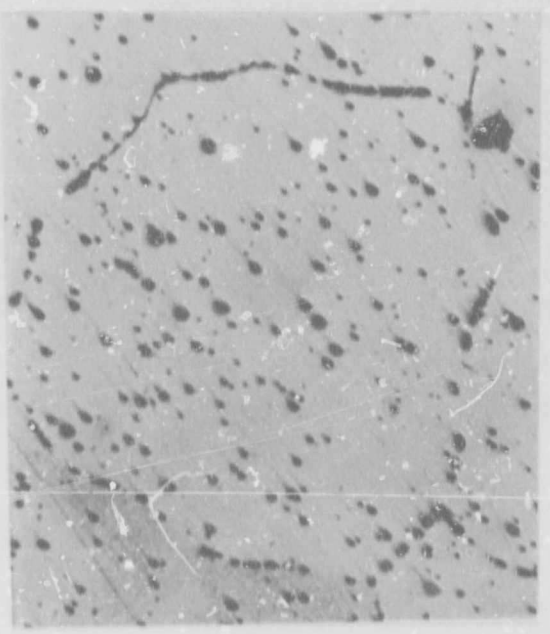


Figure 4.17 REM oxide inclusions. Section perpendicular to the rolling direction (V2/3). Glyceregia etch.

4.5.3 Sigma precipitation

The V2 and V3 series of alloy did not contain σ-phase and were found to be consistently ductile, while the original alloy (LNNI) and the V4 series in which this compound was present, were brittle. The precipitation of σ is therefore closely associated with embrittlement.

The rate of precipitation of this phase was greatly accelerated by cold work and the LNNI alloy which was rolled down to 650°C contained very thick σ stringers orientated in the rolling direction.

In the V4 alloys, σ occurred both along the annealed grain boundaries and in association with carbide stringers. The grain boundary precipitates were relatively thin and required a special etchant (which leaches σ preferentially) to expose them.

In order to recover toughness in the alloys containing σ-phase, high annealing temperatures (greater than 1050°C) were required. Even then the microstructures still contained traces in the form of fine discontinuous grain boundary films. It is clear, therefore, that in the Fe-40Cr alloys, σ is stable to temperatures much higher than the 820°C indicated on the equilibrium phase diagram.

A typical example of σ morphology and distribution in the LNNI alloy is shown in Figure 4.18. The dissolution of σ during the annealing of alloy V4/0,X at 1150°C is recorded in Figures 4.19(a to d).

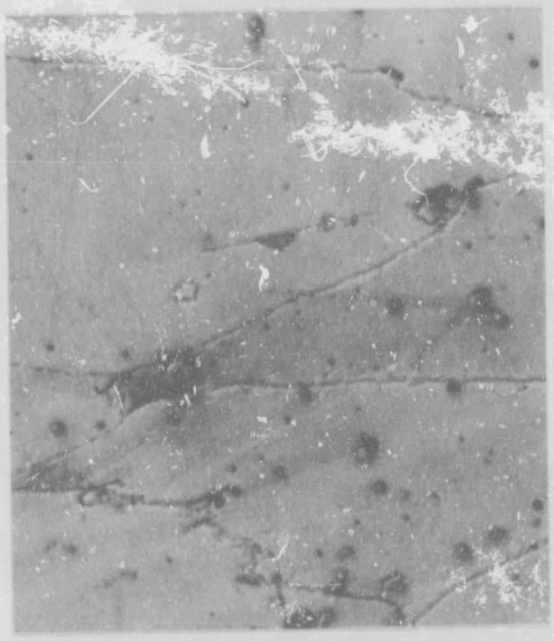
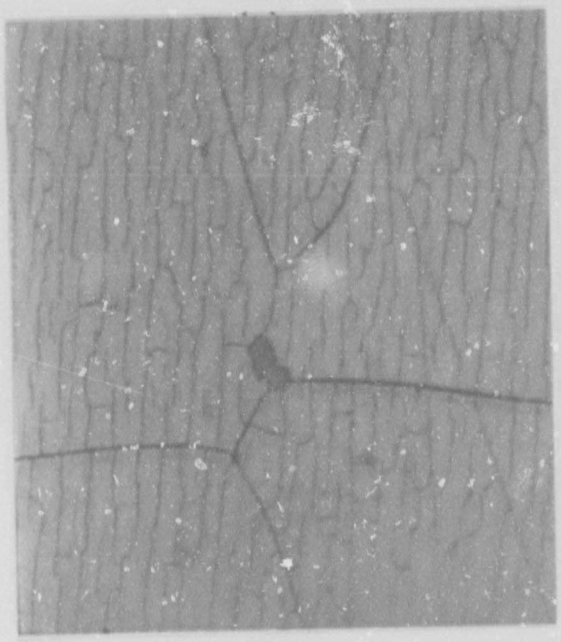


Figure 4.18 Grain boundary σ-phase in the LNNI alloy (Reduction 53%). Glyceregia etch.



10µm



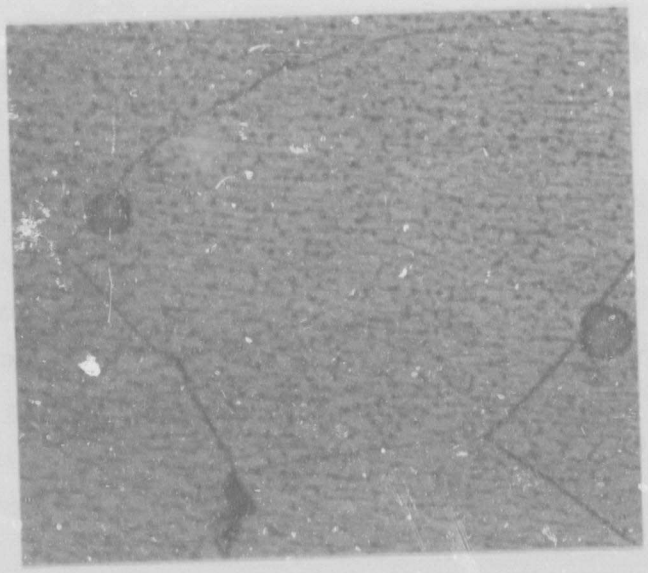
10µm

(b)

Figure 4.19 The dissolution of σ-phase during the annealing of alloy V4/0,10 at 1150°C.

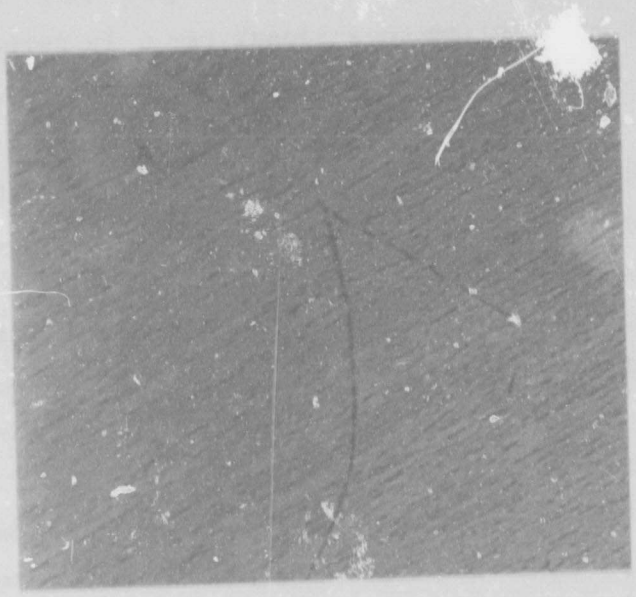
a) Grain boundary σ after 1 hour (Impact energy, 6J).

b) Grain boundary σ after 2 hours (Impact energy, 140J).



10μm

(c)



10μm

(d)

Figure 4.19 continued.

c) Grain boundary σ after 2,5 hours annealing at 1150°C (Impact energy, 140J).

d) Grain boundary σ after 3 hours at 1150°C (Impact energy, 100J).

4.5.4 Carbide precipitation

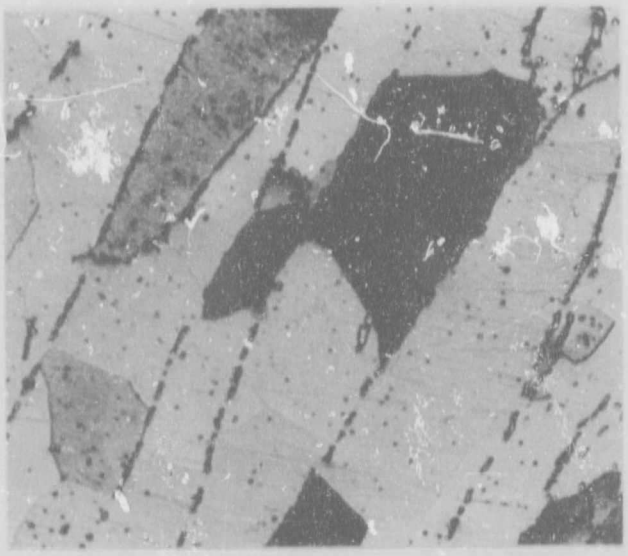
Since the carbon content of the Fe-40Cr alloys was high (as in the V4 alloys) copious and coarse grain boundary precipitation was observed (Figure 26a and b. When the alloy was rolled at temperatures at which carbon was no longer maintained in solid solution, the carbide stringers required prolonged treatment at high temperatures for dissolution, and this usually resulted in the partial restoration of ductility. In order to prevent the development of carbide stringers, low carbon materials had to be utilised (such as the V2 and V3 alloys) and low rolling temperatures avoided.

4.5.5 Slip mode and fracture initiation studies

Electropolished Charpy test specimens of the V2 and V3 alloys were examined under the light microscope after testing. The relationship between slip and fracture modes, and the involvement of twins and precipitates in fracture was investigated.

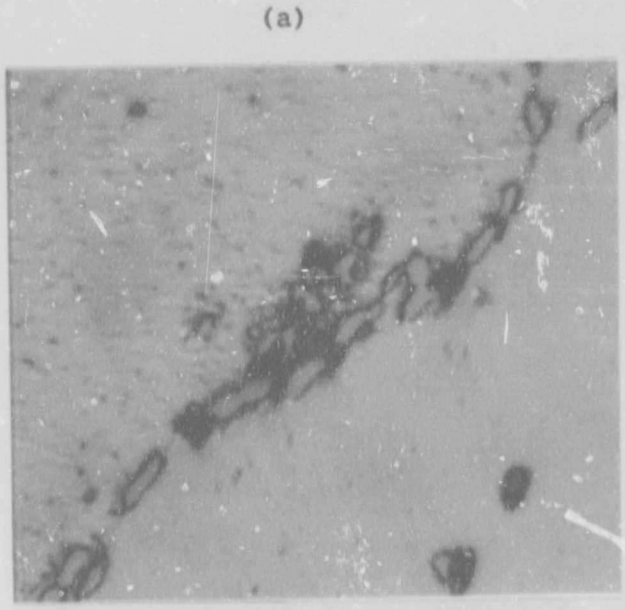
Brittle fracture was found to be associated with low temperatures rather than excessive precipitation in these alloys. When the alloy fractured in a brittle manner very little cross-slip was evident on polished surfaces (Figure 4.21). Typically, only one set of slip planes was activated within each grain. Brittle fracture also involved extensive twinning within 1mm of the fractured edge. Twins were observed impinging on grain boundaries but there was no evidence to suggest that this resulted in crack initiation (Figure 4.22). Inclusions appeared to play little role in the fracture process, since they simply separated from the matrix during fracture.

Ductile fracture involved extensive cross-slip (Figure 4.23). Twins were absent in the specimens which fractured in a ductile mode and the inclusions were observed again to have no involvement in fracture (Figure 4.24).



100μm

(a)



5μm

(b)

Figure 4.20 Grain boundary carbides in the V4/0 alloy.
a) Carbide stringers enclosing recrystallised grains. Glyceregia etch, and
b) Higher magnification showing the discontinuity of the stringers.



Figure 4.21 Typical slip associated with brittle fracture. V2/1/2 tested at -15°C.



Figure 4.22 Twins associated with the fractured edge and impinging onto a grain boundary. V2/2/2 tested at -15°C.



Figure 4.23 Extensive cross-slip associated with ductile fracture. V3/2 tested at 10°C.

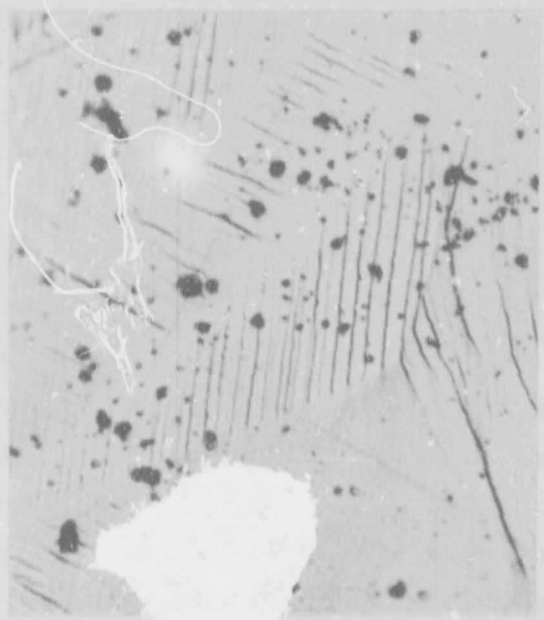


Figure 4.24 Typical field of inclusions showing no involvement is twinning or fracture. V2/2/2 tested at -15°C.

4.5 SCANNING ELECTRON MICROSCOPE

The scanning electron microscope was used in the further investigation of the effects of both twinning and precipitation on the fracture mode.

4.6.1 The V2 and V3 Alloys

Scanning electron microscopy essentially confirmed the observations made during optical examination of the electropolished surfaces:

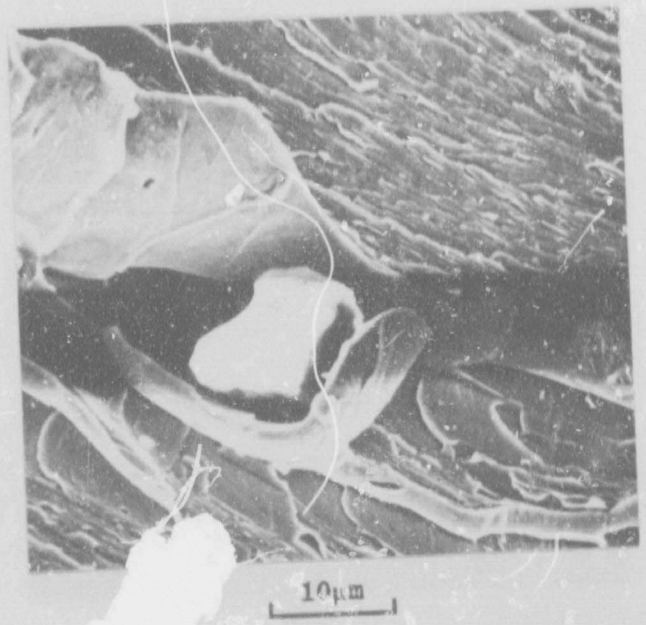
(i) inclusions are not involved in the fracture initiation process, since again it was observed that the inclusions separated from the matrix during deformation (Figures 4.25 a and b), and

(ii) fracture initiation was not associated with twinning (Figures 4.26 a and b).

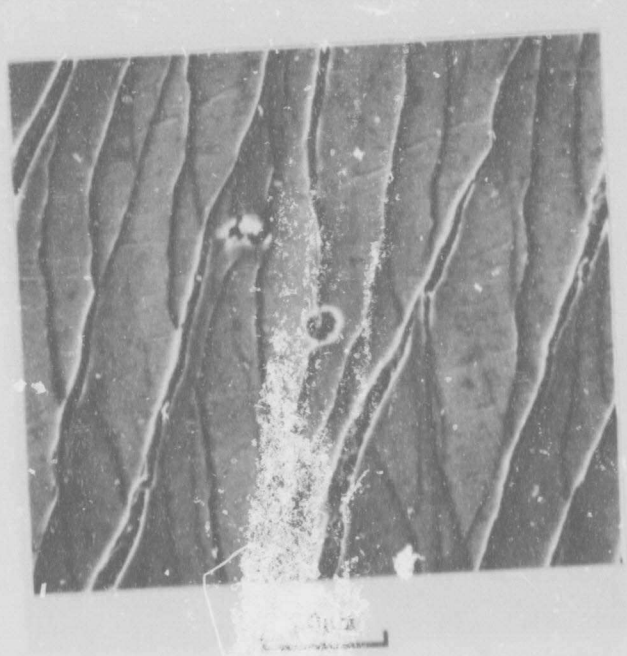
The SEM study also yielded additional information on the mode of fracture. No fully intergranular brittle fracture surfaces were observed and these usually consisted of mixtures of cleavage and intergranular fracture (Figure 4.27). Although the ductile fractures exhibited the classic fibrous and dimpled appearance, small areas of cleavage were common (Figure 4.28).

4.6.2 The V4 alloys

The V4 alloys were characterised by extensive grain boundary precipitation. Many twins were observed impinging on the grains boundaries (Figure 4.29). Some of these twins were cracked and associated with local tearing of the grain boundary (Figure 4.30). Cracks were also seen to initiate from grain boundary precipitates (Figure 4.31 a and b). All these phenomena were observed in both ductile and brittle alloys.



(a)



(b)

Figure 4.25 Separation of the inclusions from the matrix during fracture

a) Brittle fracture surface. Alloy (V2/1/2 tested at -15°C).

b) Ductile fracture. (Alloy V3/2 tested at 36°C.) Note tearing along the cleavage planes.



5µm

(a)



5µm

(b)

Figures 4.26 Twins showing no involvement in fracture.
a) Twin impinging on a grain boundary. (Alloy V3/2 tested at -20°C.)
b) Twins close to the fracture edge. (Alloy V3/2 tested at -20°C.)



Figure 4.27 Brittle fracture surface - a mixture of cleavage and intergranular fracture. (Alloy V2/2/2 tested at 0°C.)

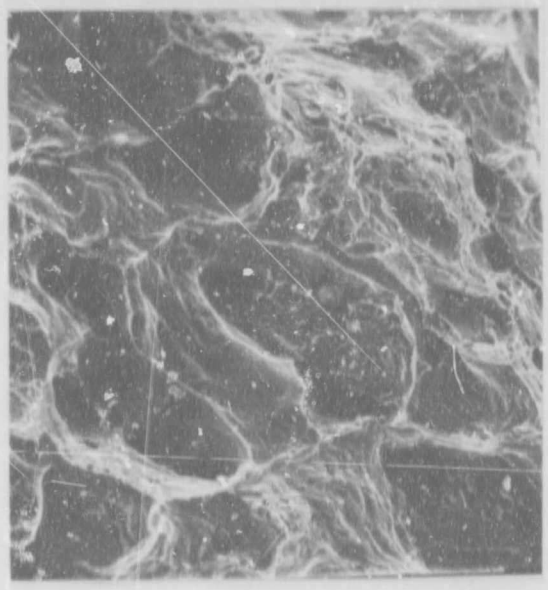


Figure 4.28 Fracture showing ductile tearing and areas of cleavage. (Alloy V3/2 tested at ambient temperature.)

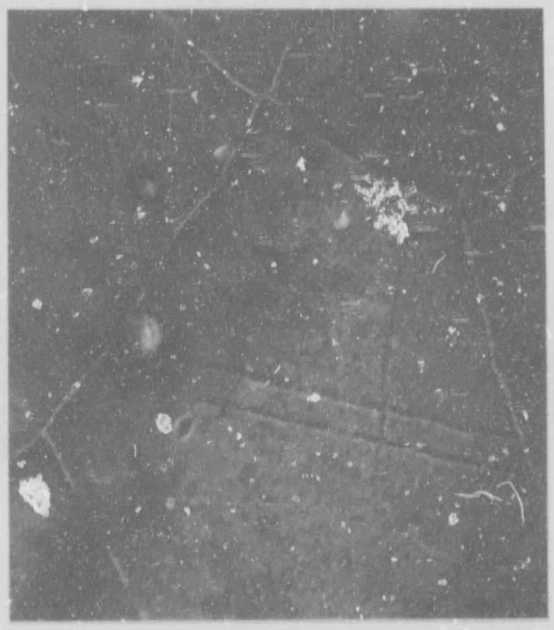


Figure 4.29 Twin impinging on grain boundary precipitates. The round inclusion is a REM oxide. (Alloy V4/0,10, embrittled.)

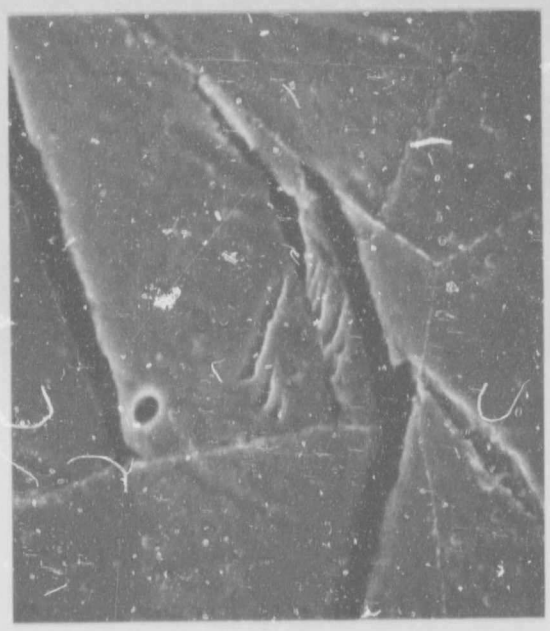
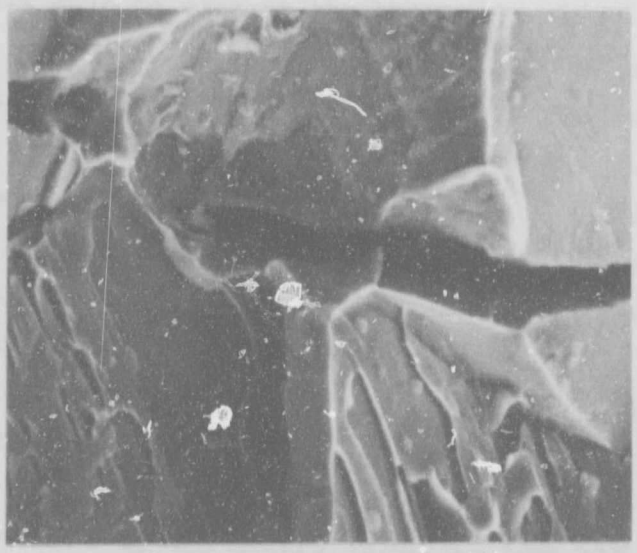
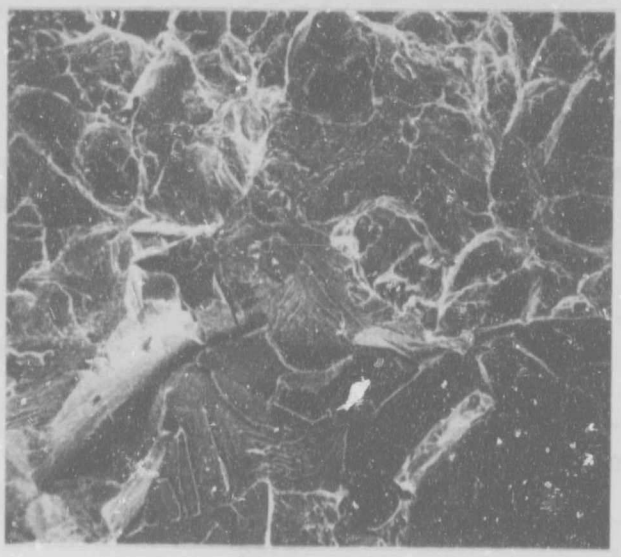


Figure 4.30 Twin associated with tearing at the grain boundary. (Alloy V4/0,10, ductile.)



10μm

(a)



50μm

(b)

Figure 4.31 The involvement of grain boundary precipitates in the fracture of the V4 alloys.
a) Crack initiated from grain boundary precipitates (Alloy V4/0).
b) Cracking along the grain boundary associated with precipitation (Alloy V4/0,10).

An attempt was made to measure the thickness of the grain boundary precipitates in the V4 alloys in order to determine whether this had a direct influence on fracture behaviour. This hypothesis is discussed in the next section. In the embrittled alloys the grain boundary precipitates were 1 to 1,5 µm thick, and in the ductile alloys: 0,25 to 0,5 µm thick. Typical micrographs of the grain boundary precipitation are shown in Figure 4.32 (a and b). In all cases, although ther appears to be a tendency toward grain boundary film formation, the precipitates remain relatively discontinuous.

4.6.3 Energy dispersive spectrometry (EDS) in the SEM

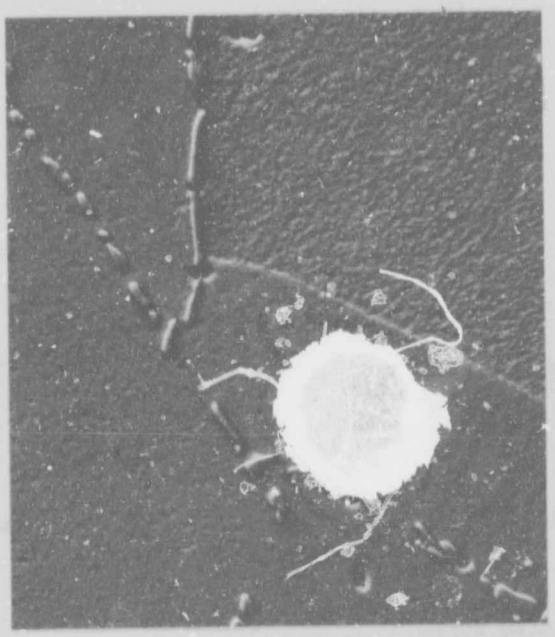
EDS analysis was carried out on the precipitates at the boundaries of the rolled grains in alloy V4/0. It showed that these precipitates have a much higher Cr:Fe ratio than the matrix (Figures 4.33 and 4.34). The combined weight % of iron and chromium, however, fell short of 100% and computation by stoichiometry showed that if the outstanding amount was made up by carbon, the analysis would correspond to the formula of the $M_{23}C_6$ carbide. The EDS results are given in Table 4.12.

Table 4.12 Results of EDS analysis of the rolled grain boundary precipitates in alloy V4/0.

Element	Weight %	% error
Cr	55,57	1,12
Fe	26,96	0,87
C	17,70	*
TOTAL	100,23	

* C computed by stoichiometry

It was thus concluded that the precipitates were probably $M_{23}C_6$ carbides and TEM work was performed in an attempt to provide conclusive confirmation.



10μm

Figure 4.32 Grain boundary carbides which occur as discontinuous carbide stringers in alloy V4/0.

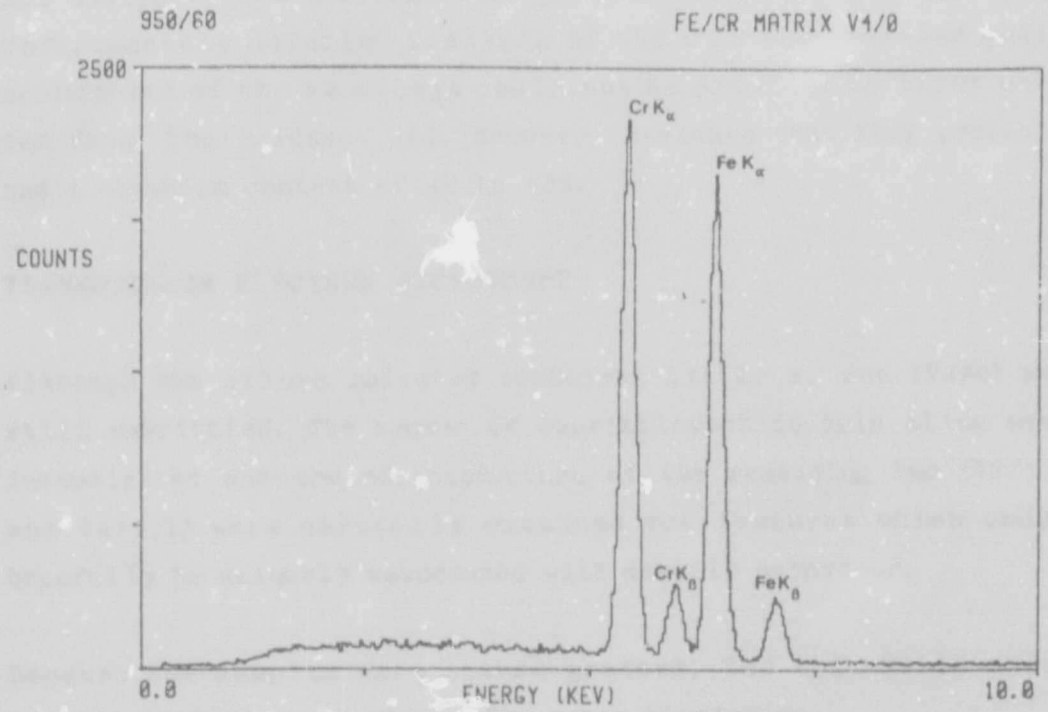


Figure 4.33 Spectrograph of Fe-40Cr matrix

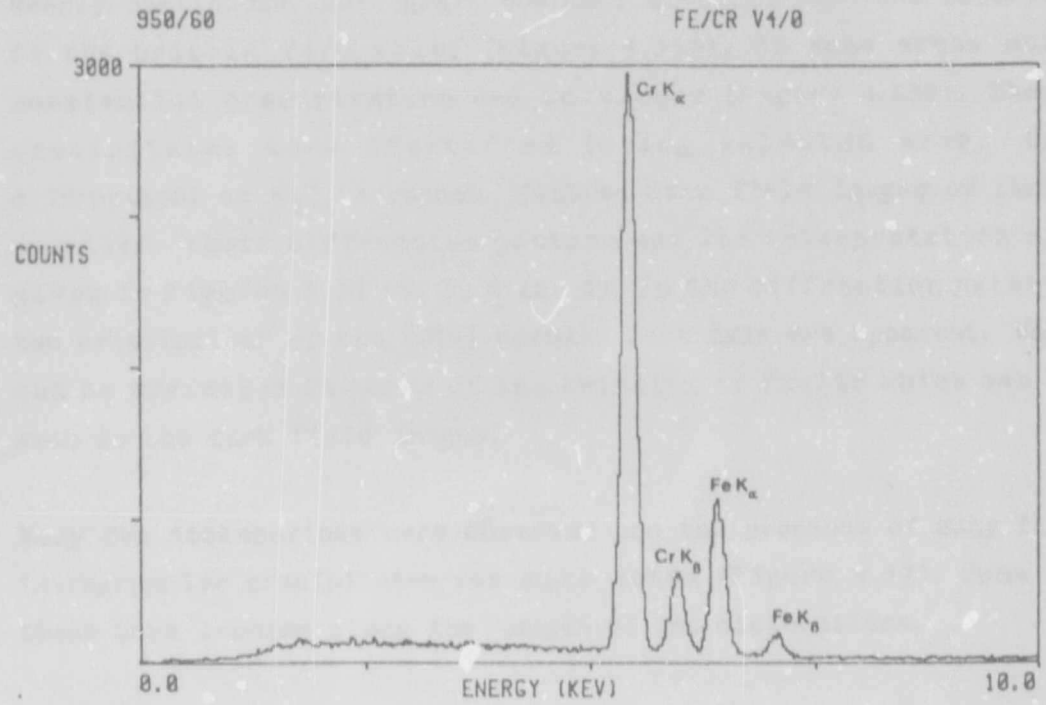


Figure 4.34 Spectrograph showing the iron and chromium content of the carbide precipitates.

Author Hermanus Mavis Ann
Name of thesis The development of a tough high chronmium ferritic stainless steel. 1986

PUBLISHER:

University of the Witwatersrand, Johannesburg
©2013

LEGAL NOTICES:

Copyright Notice: All materials on the University of the Witwatersrand, Johannesburg Library website are protected by South African copyright law and may not be distributed, transmitted, displayed, or otherwise published in any format, without the prior written permission of the copyright owner.

Disclaimer and Terms of Use: Provided that you maintain all copyright and other notices contained therein, you may download material (one machine readable copy and one print copy per page) for your personal and/or educational non-commercial use only.

The University of the Witwatersrand, Johannesburg, is not responsible for any errors or omissions and excludes any and all liability for any errors in or omissions from the information on the Library website.